



A Multiscale Model for Recruitment Aggregation of Platelets by Correlating with *In Vitro* Results

PRACHI GUPTA,¹ PENG ZHANG,² JAWAAD SHERIFF,² DANNY BLUESTEIN,² and YUEFAN DENG¹

¹Department of Applied Mathematics and Statistics, Stony Brook University, Stony Brook, NY 11794-3600, USA; and
²Department of Biomedical Engineering, Stony Brook University, Stony Brook, NY 11794, USA

(Received 22 December 2018; accepted 26 June 2019; published online 9 July 2019)

Associate Editor Michael R. King oversaw the review of this article.

Abstract

Introduction—We developed a multiscale model to simulate the dynamics of platelet aggregation by recruitment of unactivated platelets flowing in viscous shear flows by an activated platelet deposited onto a blood vessel wall. This model uses coarse grained molecular dynamics for platelets at the microscale and dissipative particle dynamics for the shear flow at the macroscale. Under conditions of relatively low shear, aggregation is mediated by fibrinogen via α IIB β 3 receptors.

Methods—The binding of α IIB β 3 and fibrinogen is modeled by a molecular-level hybrid force field consisting of Morse potential and Hooke law for the nonbonded and bonded interactions, respectively. The force field, parametrized in two different interaction scales, is calculated by correlating with the platelet contact area measured *in vitro* and the detaching force between α IIB β 3 and fibrinogen.

Results—Using our model, we derived, the relationship between recruitment force and distance between the centers of mass of two platelets, by integrating the molecular-scale inter-platelet interactions during recruitment aggregation in shear flows. Our model indicates that assuming a rigid-platelet model, underestimates the contact area by 89% and the detaching force by 93% as compared to a model that takes into account the platelet deformability leading to a prediction of a significantly lower attachment during recruitment.

Conclusions—The molecular-level predictive capability of our model sheds a light on differences observed between transient and permanent platelet aggregation patterns. The model and simulation framework can be further adapted to simulate initial thrombus formation involving multiple flowing platelets as well as deposition and adhesion onto blood vessels.

Keywords—Multiscale modeling, Hybrid force field, Contact area, Detaching force.

INTRODUCTION

Cardiovascular diseases account for 31% of all deaths globally and in US, annually.¹ Whether due to acute thrombosis associated with myocardial infarction, or progressive intermittent atherothrombotic events, significant ventricular dysfunction may result, leading to heart failure. Thrombosis in vascular disease is potentiated by interactions of blood constituents with an injured vascular wall and non-physiological flow patterns characterizing cardiovascular pathologies. It has been recognized that through the complex and dynamic process of aggregation platelets play a significant role in thrombus formation that may lead to cardiovascular diseases.

Aggregation is the “cohesion” of platelets to each other and to the thrombogenic surfaces.¹⁶ At low-intermediate shear, as commonly occurs in veins and larger arteries, aggregation is predominantly mediated by α IIB β 3 on free-flowing platelets which engage fibrinogen (Fg) adsorbed on platelet monolayers, composing the initial thrombi. Aggregation is mediated by several factors including glycoprotein receptors, their ligands, and shear stress acting as a stimulus.^{16,17,23,28}

The distinct aggregation phenomena such as tether formation,²³ reversible and stable aggregation,²³ filopodia formation,⁷ and aggregation without perceptible shape change or filopodia formation was studied extensively during the past decades.^{7,16,17,23,28}

Each of the above phenomena are mediated by diverse flow conditions and involve participation of different glycoprotein receptors and their ligands. Aggregation at low shear levels occurs through the interactions of fibrinogen with integrin α IIB β 3. Pathological flow conditions can affect the process of thrombus formation by altering the dynamics of α IIB β 3–Fg binding.^{2,34}

These observations motivate the investigation of the

Address correspondence to Yuefan Deng, Department of Applied Mathematics and Statistics, Stony Brook University, Stony Brook, NY 11794-3600, USA. Electronic mail: Yuefan.Deng@StonyBrook.edu

mechanical response of platelets to such flow conditions.

Aggregation leading to thrombus formation has been an intriguing phenomenon and has attracted remarkable attention from modelers in the past.^{6,13–15,19,26,27,30,31,41,42,45} A few different approaches have been used to model aggregation and disaggregation phenomena. Continuum multiscale models for aggregation^{26,27} and thrombus formation⁴⁵ examined the role of flow conditions, platelet's position in the flow and the receptor–ligand bond in aggregation. Though the approach can accommodate the platelet shape and proximity to the wall for characterizing the aggregation properties, it cannot simulate the interactions of the receptors at the microscale. DPD-PDE-based hybrid methods for studying platelet aggregation^{41,42} neglected the receptors and thus incapable of capturing such microscale phenomena. Common to all these models was treating platelets as rigid particles because of platelet's much higher stiffness as compared to red blood cells (RBCs), likely underestimating the contact properties during aggregation.

At smaller scales, such as in microcirculation, blood shows complex rheological behavior which leads to the migratory behavior of smaller cells. During margination, RBCs in the core flow push smaller constituents like platelets to the periphery, forming a cell-depleted layer. This peripheral cell-depleted layer has lower viscosity compared to the RBC core. This unique property has been utilized in our own *in vitro* experiments, in which platelets forced to the periphery of the microchannel adhere to immobilized vWF and begin the process of recruitment.

It has been demonstrated by two research groups^{16,23,36} that under certain shear flow conditions, platelet aggregation occurs without visible platelet shape change and filopodia formation. Under conditions of low shear stress below 10 dyne/cm², the receptor α IIB β 3 and the fibrinogen form a bridge (α IIB β 3–Fg– α IIB β 3) which initiates platelet aggregation without visible shape change.²³ Therefore, the first phase of our modeling considers aggregation without activation where platelets retain their discoid shape and do not have filopodia.

Using DPD to describe the viscous flow and CGMD to describe the intra-platelet constituents, we constructed a multiscale model for platelets in viscous flows.⁴⁶ This model allowed us to study the mapping of hemodynamic shear stresses on platelet membrane surface and platelet dynamics in flow like flipping. We extended this model to a platelet model⁴⁸ with 140,015 particles and validated the intra-platelet components (which constitute the bilayer platelet membrane, gel like cytoplasm and intra-platelet cytoskeleton) properties with the published *in vitro* experiments. This

multiscale platelet model continuously changes its morphology in response to the dynamic flow stresses.^{46,48} However, these models did not include yet receptors and associated inter-platelet force fields required for modeling aggregation.

We extended the previous efforts to study, and accurately reproduced, the properties of recruitment aggregation by incorporating the role of receptors at the molecular scale. We formulate a hybrid force field based on Morse potential for modeling the long-medium range interactions and harmonic potential for modeling α IIB β 3–Fg– α IIB β 3 bond formation between the platelets. The Morse potential has been used to model intercellular interactions for red blood cell aggregation,⁴⁷ to simulate binding of GPIb and vWF,³⁸ and to model thrombus formation.⁴⁵ Since platelet aggregation involves an initial contact and then bonding two α IIB β 3 receptors to an Fg molecule, the hybrid force field incorporates both the coarse-grained initial contact and the fine-grained binding between the receptors.

We validated our recruitment aggregation simulations with *in vitro* measurements of contact area and detaching force of platelets flowing in microchannels and predicted quantities such as recruitment force, approach speed and minimum distance between two platelets, which are very challenging to measure *in vitro*. Utilizing our deformable model, a formula for recruitment force as a function of the distance between platelet centers is introduced for the first time, and the inaccuracies stemming from treating the platelets as rigid are demonstrated.

MULTISCALE MODELING

Following our previous work,^{8,46,48} our multiscale model uses DPD for simulating the top scale macroscopic shear flow and CGMD (Coarse Grained Molecular Dynamics) for the mesoscopic bottom scale of the molecular model of platelets.^{8,46} Each DPD particle embodies a cluster of atoms or molecules and their collective motion is governed by following^{4,11}:

$$dv_i = \frac{1}{m_i} \sum_{j \neq i}^N (\mathbf{F}_i^C dt + \mathbf{F}_i^D dt + \mathbf{F}_i^R \sqrt{dt} + \mathbf{F}_i^E dt) \quad (1)$$

where

$$\mathbf{F}_i^C = a \left(1.0 - \frac{r_{ij}}{r_c} \right) \mathbf{e}_{ij},$$

$$\mathbf{F}_{ij}^D = -\gamma \omega^D(r_{ij}) (\mathbf{e}_{ij} \cdot \mathbf{v}_{ij}) \mathbf{e}_{ij},$$

$$\mathbf{F}_{ij}^R = \sigma \omega^R(r_{ij}) \zeta_{ij} \mathbf{e}_{ij},$$

$$\omega^D(r_{ij}) = [\omega^R(r_{ij})]^2 = \left(1.0 - \frac{r_{ij}}{r_c}\right)^{2k}$$

where F^C , F^D , F^R are conservative, dissipative and random forces acting on the particle and F^E is the external force exerted to each particle to lead the fluid flow. r_{ij} is the inter-particle distance $\mathbf{v}_{ij} = \mathbf{v}_i - \mathbf{v}_j$, is the relative velocity and \mathbf{e}_{ij} is a unit vector in the direction $\mathbf{r}_i - \mathbf{r}_j$. ζ_{ij} is the standard Gaussian random variable with zero mean and unit variance, α is the maximum inter-particle repulsion given by $\alpha = 75k_b T / (\rho_f r_c)$ where ρ_f is the number of fluid particles. Español *et al.*⁴ established a relation between and and weight functions given by $\sigma^2 = 2\gamma k_B T$, $k_B T = 1.0$.

We use the DPD method described above with parameters $a = 25.0$, $\gamma = 67.5$, $k = 0.25$, $r_c = 1.7^8$ to achieve force-driven viscous shear flow in straight microchannel of dimensions $35.6 \times 16 \times 35.6 \mu\text{m}$. The dynamic viscosity of the flow is 1.07 mPa s . We implement periodic boundary conditions in x and z dimensions. In y dimension no-slip boundary condition between the flow and the vessel wall is imposed as previously described by us.⁴⁰ This general no-slip condition consists of the generation of fictitious particles by reflecting flow particles across the vessel wall (constructed with triangular plane) with inverted velocity to develop an equilibrated shear layer across the microchannel wall, thereby imposing zero velocities at the wall plane.^{40,44}

CGMD potential is given by

$$V_{\text{CGMD}} = \sum_{\text{bonds}} k_b (r - r_0)^2 + \sum_{L-J} 4\epsilon_{ij} \left[\left(\frac{\sigma_{ij}}{r}\right)^{12} - \left(\frac{\sigma_{ij}}{r}\right)^6 \right], \quad (2)$$

where k_b is the force constant, ϵ_{ij} is the well depth of the Lenard Jones (L-J) potential and σ_{ij} is the finite distance and r is the interparticle distance.

As described in our previous work⁴⁸ the first term in Eq. (2) describes the deformability of the membrane.¹⁸ Young's modulus for our membrane is $(1.5 \pm 0.6) \times 10^3 \text{ dyne/cm}^2$.⁴⁶ To compare, the Young's modulus for human platelet is $(1.7 \pm 0.6) \times 10^3 \text{ dyne/cm}^2$.¹² The second term describes the interaction between membrane and the intercellular particles. The bond energy between two adjacent membrane particles is given by $k_b = 2.54 \times 10^{-3} \text{ kcal/mol/\AA}^2$ and $r_0 = 42.7 \text{ nm}$. Departing from a rigid platelet model and using this model to study aggregation allowed us to study the impact of platelet deformability during recruitment aggregation.

The DPD–CGMD methods are spatially interfaced at the platelet membrane surface using the following hybrid force field⁴⁶

$$d\mathbf{v}_i = \frac{1}{m_i} \sum_{j \neq i}^N (\nabla U_{LJ}(r_{ij}) dt + \mathbf{F}_{ij}^D \sqrt{dt} + \mathbf{F}_{ij}^R dt), \quad (3)$$

where $U_{LJ} = 4\epsilon \left[\left(\frac{\sigma}{r_{ij}}\right)^6 - 2\left(\frac{\sigma}{r_{ij}}\right)^{12} \right]$, $\mathbf{F}_{ij}^D = -\gamma \omega^D(r_{ij}) (\mathbf{e}_{ij} \cdot \mathbf{v}_{ij}) \mathbf{e}_{ij}$ and $\mathbf{F}_{ij}^R = \sigma \omega^R(r_{ij}) \zeta_{ij} \mathbf{e}_{ij}$. ϵ and σ are the characteristic energy and distance parameters in CGMD. Other parameters including γ and σ have the same definitions as in DPD. All forces are truncated beyond a cutoff radius which defines the length scale in the fluid-platelet contact region.⁵

The L–J force maintains the cytoskeleton-confined shapes and the incompressibility of the platelets against the applied stress of the surrounding flow. The dissipative and random force terms simulate interactions between the flow and platelet through exchange of momentum which preserves local thermodynamic and mechanical properties. No-slip boundary condition is imposed on the platelet membrane through this intricate repulsive-drag force. The dissipative forces of the membrane particles drag the flow particles thereby reproducing boundary layer mechanism where adjacent layers are dragged by one another. At the same time, the L–J force provides a repulsive force thus preventing the flow particles from penetrating through the platelet membrane.⁴⁶

Using the above methodologies, we have a platelet model immersed in DPD fluid in which the microstructural changes of platelets respond to the extracellular viscous shear stresses transferred to them. Since the platelet membrane is allowed to deform, it enables deformability in response to such mechanical stresses. The interaction between the two systems preserves dynamic properties of the flowing platelets, such as the flipping motion.⁴⁶

In this work, we study the recruitment aggregation in which flowing platelet undergoes aggregation through binding of Fg adsorbed on the surface of an adhered platelet mediated by $\alpha\text{IIb}\beta_3$. There are 80,000–100,000 $\alpha\text{IIb}\beta_3$ receptors on a typical platelet surface²⁴ that serve as a physical connector between fibrinogen and the platelet cytoskeleton.^{16,23,34} To reduce the computational cost, we use DPD to simulate plasma flow and the recruitment of marginated platelet is considered by using Morse potential, assuming that platelets are already marginated towards the vessel wall to the cell free layer characteristic of plasma flow in the microcirculation. Figure 1, shows a complete picture of our model setup. Our model consists of two

platelets in Poiseuille viscous shear flow in a microchannel. We assume that the platelets have margined and entered the cell free layer. We consider homotypic interactions in which one platelet is adhered to the lower wall of the microchannel and the flowing platelet is recruited to it leading to aggregation. A platelet is modeled as a discoid shaped spheroid with a $2 \mu\text{m}$ semi-major axis and $0.5 \mu\text{m}$ semi-minor axis.⁴⁸ At the fluid-platelet interface, the membrane prevents fluid particles from penetrating while maintaining the flowing platelet flipping dynamics.³³ In low-intermediate shear flows aggregation requires $\alpha\text{IIb}\beta3$ and ligand Fg binding and can occur independent of shape change.²³ Each platelet includes 67,004 $\alpha\text{IIb}\beta3$ receptors²⁴ represented by particles and distributed uniformly on the membrane. Receptor density on the platelet surface is $2342 \text{ particles}/\mu\text{m}^2$.

THE AGGREGATION MODEL

Recruitment aggregation undergoes diverse phases until forming a stable aggregate. The aggregation model developed here is capable of modeling recruitment in the cell-free layer and aggregation at the microscales. This multiscale process requires a hybrid force field that precisely describes the interaction between platelets. We present an interplatelet force

field and its parametrization for recruitment aggregation.

The Interplatelet Force Field

We construct an electrical-neutral molecular-scale force field that can efficiently yield the properties of recruitment aggregation. To mimic the dynamic binding of the receptors during aggregation we use a harmonic term.^{41,42} At the same time, we use a Morse term in the force field to mimic the long-medium range effect of aggregation.⁴⁵ So, the functional expression for molecular dynamics potential is represented by

$$U_{\text{total}} = U_{\text{bonded}} + U_{\text{nonbonded}}, \quad (4)$$

where

$$U_{\text{bonded}} = \sum_{\text{bonds}} \frac{f^A}{2r_0} (r - r_0)^2$$

and

$$U_{\text{nonbonded}} = \sum_{\text{neighbors}} D_0 \left(e^{-2\alpha(r-r_0)} - 2e^{-\alpha(r-r_0)} \right),$$

where r is the distance between two particles and r_0 is the equilibrium bond length, D_0 is the well depth, α is the scaling factor, r_0 is the equilibrium bond length $\mathbf{r}_{ij} = \mathbf{r}_i - \mathbf{r}_j$, $r_{ij} = |\mathbf{r}_{ij}|$, $\mathbf{e}_{ij} = \mathbf{r}_{ij}/r_{ij}$ and f^A is the force

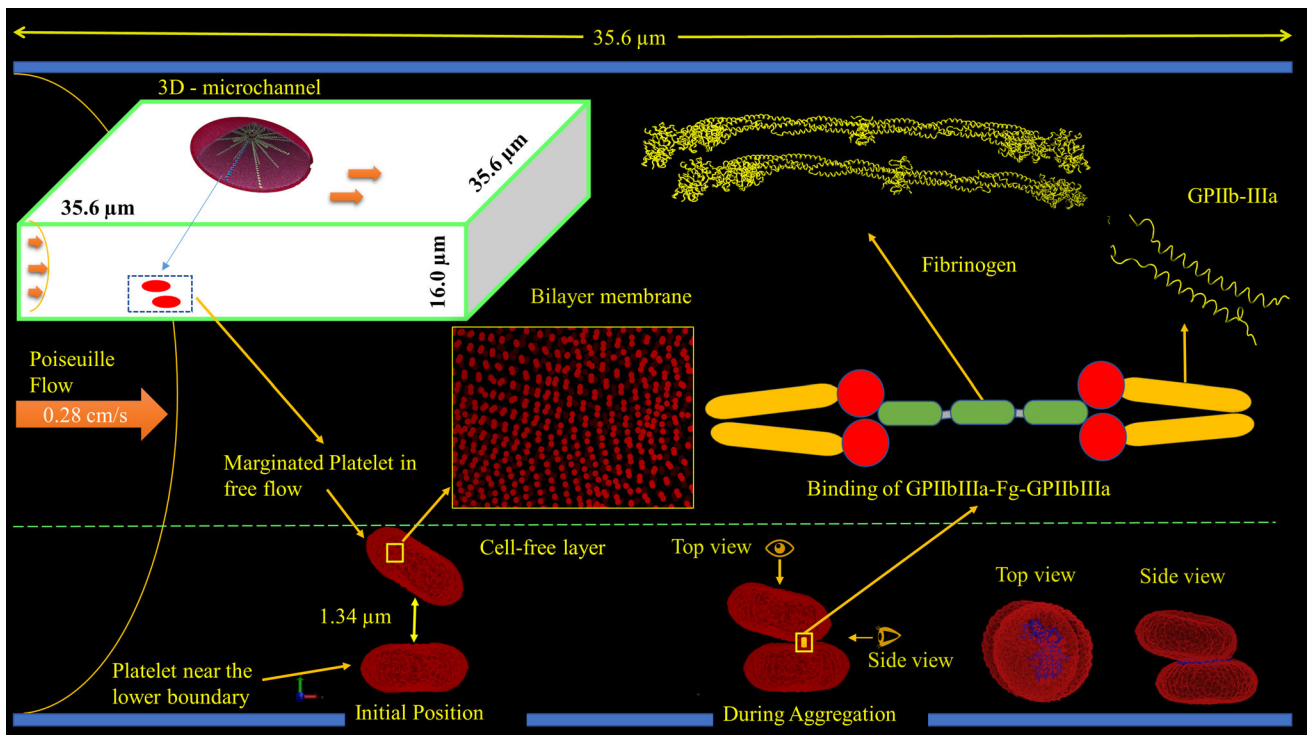


FIGURE 1. Schematic model representation.

strength coefficient. Differentiating the potential, the hybrid force field is written as:

$$\mathbf{F}_{ij} = \left(2\alpha D_0 \left(e^{-2\alpha(r_{ij}-r_0)} - e^{-\alpha(r_{ij}-r_0)} \right) + f^A \left(1 - \frac{r_{ij}}{r_0} \right) \right) \mathbf{e}_{ij} \quad (5)$$

We performed an initial analysis of the force field to assess its effect on recruitment aggregation characteristics. The Morse term in the force field consists of (i) an attractive part $\left(-e^{-\alpha(r_{ij}-r_0)} \right)$ that contributes to aggregation by initiating and enhancing bond formation and (ii) a repulsive part $\left(e^{-2\alpha(r_{ij}-r_0)} \right)$ that prevents the membrane particles from overlapping during aggregation. The parameter r_0 represents the force relaxation distance, F_{ij} is repulsive when $r_{ij} < r_0$ and attractive when $r_{ij} > r_0$.

To adapt the force field Eq. (5) for modeling aggregation at microscales we use the bond length of $r_0 = 0.38$ which is the equilibrium bond length of $\alpha\text{IIb}\beta 3\text{-Fg-}\alpha\text{IIb}\beta 3$ (67.5 nm)¹⁰ in dimensionless units. To determine the cutoff (r_c) for aggregation we use the approximate distance between platelet surface when a bond can begin to form. The $\alpha\text{IIb}\beta 3$ receptors extend about 20 nm above the surface^{29,43} and Fg is about 47.5 nm in molecular length,²⁰ the approximate distance between platelet surface for aggregation to begin is 87.5 nm. The undetermined parameters α , D_0 and f^A which control the forces between the two platelets are further determined by correlating with contact area measured from the *in vitro* experimental images (see details in “*In Vitro* Experiments”).

Parameter Determination

With the formula for aggregation force constructed (“*The Interplatelet Force Field*”), we proceed to the next step, i.e., determining the values of the parameters. Using the interplatelet force field we performed a series of numerical experiments to understand the dependencies and sensitivities of the parameters in the force field on platelet aggregation. We determine the values of the parameters in the interplatelet force field by correlating simulation results with *in vitro* results. We design this in three steps. Step 1, determining the values for r_0 and r_c from the molecular level details such as the equilibrium bond length and length of $\alpha\text{IIb}\beta 3$ extension from the platelet surface. Step 2, performing coarse grained tuning of the parameters (α and D_0) in the Morse term. Step 3, fine grained tuning of parameter (f^A) in Hooke’s term. Having described the first step at the end of “*The Interplatelet Force*

Field” we present the rationale and details of the second and third steps in the following paragraphs.

Coarse-Grained Tuning Using Contact Area

The trajectory of the approaching recruited platelet to the already deposited platelet is governed by the Morse term in the force field, whereas the bond formation between the receptors is from the Hooke’s term in the force field. We therefore begin this process by coarse grained tuning of the parameters that affect contact position using the rigid platelet model and then proceed to fine grained tuning of the parameter that directly relates to the $\alpha\text{IIb}\beta 3\text{-Fg}$ bond based on molecular level details in “*Fine-Grained Tuning Using Detaching Force*”. Since α controls the well width of the potential, any change in the value of α significantly affects the trajectory of the approaching platelet and hence affects the eventual conferred contact between platelets.

Using the rigid platelet model, we determine the range for $\alpha \in [0.8, 1.2]$ with $D_0 = 10.0$. The lower limit for α is determined because when $\alpha < 0.8$ the interplatelet force becomes too strong and cannot maintain the correct thermodynamic properties (temperature is not stable and increases to 5.99 in DPD units). With the increase in α value the contribution from the repulsive part $\left(e^{-2\alpha(r_{ij}-r_0)} \right)$ in the Morse term of the force field becomes stronger. This leads to an effective repulsive interplatelet effect leading to a decrease in contact area. So, for $\alpha > 1.2$, the contact area keeps decreasing with increase in α . In Fig. 2, we present the mean contact area for three different values of α . We observe two important aspects of modeling aggregation using the rigid platelets. First, the rigid platelet model fails to predict the contact area observed in the experiments—underestimating it by 89%. Second, contact area is influenced by change in α value and the relationship is depicted in Fig. 2. Further investigation into the force field reveals that a higher value of α not

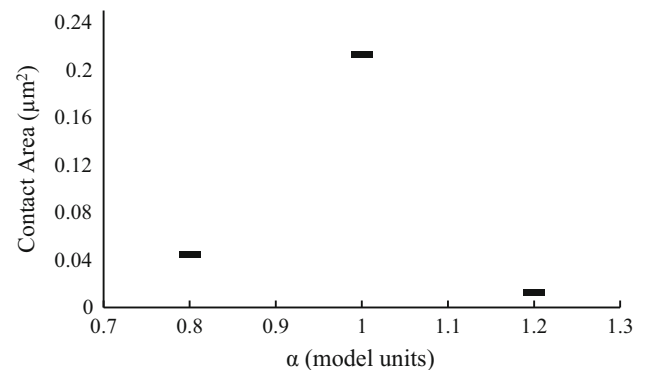


FIGURE 2. Mean value of contact area (μm^2) during the stable state of aggregation against the simulated time (μs).

only provides a higher attractive force but also increases the repulsive force which works towards decreasing the effective contact area. Therefore, determination of the α value becomes an optimization problem of the attractive and repulsive parts of the Morse term in the force field.

The numerical results agreed with the above analysis and the efficacy of this optimization approach is clearly demonstrated in Fig. 2. After finding the optimal value for α we proceed to determine D_0 . However, increasing D_0 increases the force magnitude which does not maintain the integrity of the model. Therefore, after finishing the process for coarse grained parametrization we find that the optimal values for $\alpha = 1.0$ and $D_0 = 10.0$, respectively.

Fine-Grained Tuning Using Detaching Force

Using the optimal values from the coarse-grained parametrization we then proceed to the next step for fine grained tuning of f^A using detaching force between the platelets. This requires tuning the α IIB β 3-Fg bond strength in the aggregation model, for which we utilize the deformable platelet model. We use previously published rupture forces between α IIB β 3 and Fg²¹ to calculate the detaching force (details in “Measures and Formulas”). Figure 3 presents the detaching force for four different values of $f^A \in \{0.1, 1.0, 10.0, 100.0\}$ and the range of detaching force highlighted using a grey band. It is clear that $f^A = 10.0$ provides the correct rupture force.

NUMERICAL SIMULATIONS

Simulation Settings

All simulations were performed with NVE ensemble, using LAMMPS (Large-scale of Atomic/Molecular Massively Parallel Simulator) code³² with some

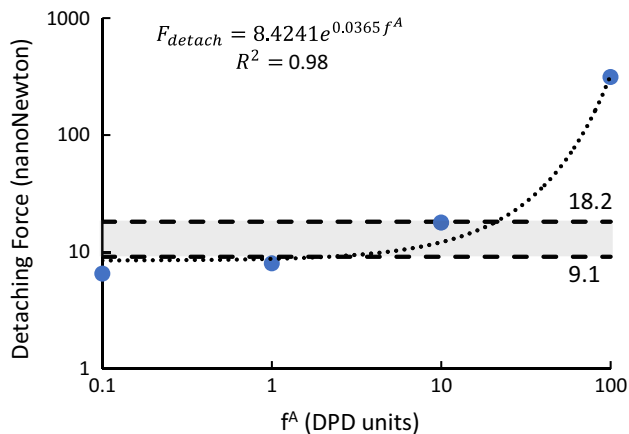


FIGURE 3. Detaching force (nanoNewton) vs. model parameter f^A .

added algorithms like no-slip boundary condition,⁴⁰ DPD-CGMD hybrid potential for interactions between platelets and flow⁴⁶ and hybrid DPD-Morse potential for reducing compressibility of the flow.⁸ The setup for our model is presented in Fig. 1. In our simulations, a typical blood viscous Poiseuille flow was employed in a microchannel of length (L) 35.6 μm , height (H) 35.6 μm and width (W) 16.0 μm . We consider platelets in a cell-free layer (marginated), and each platelet was modeled as an ellipsoid with 140,303 particles with dimension $4 \times 4 \times 1$ in μm .⁴⁸ Our multiscale platelet model continuously changes its morphology in response to the dynamic flow stresses while flowing and flipping. For modeling rigid platelets, we use LAMMPS fix rigid command. The rigid platelet model adapts the same platelet model with a rigid constraint. The total force on a rigid platelet is calculated as the sum of forces on the individual constituents and the positions, velocities, and orientations of the constituent particles are updated every time step so that the platelet moves as a single entity. The number density for fluid is 3.0. The fluid flow was driven in x-direction using a body force $g_x = 0.002$. Periodic boundary condition was employed in x and z direction. We followed⁴⁰ to implement a no slip boundary condition on the wall in the y direction. The integration timestep size reported is 2.5×10^{-5} (Table 1). We run the simulations until stable aggregation is reached and there is no significant change in contact area. Physical quantities in dimensionless units were further converted into physical units for the interpretation of aggregation and flow properties. The wall shear stress is 6.7 dyne/cm² and shear rate is 619 s⁻¹ with a flow viscosity of 1.07 mPa s.

The ability of platelet membrane receptor α IIB β 3 to associate with Fg, thus triggering recruitment aggregation of unactivated platelets,¹⁶ makes it crucial to measure the interaction between platelet membrane receptors. We conducted accordingly simulations to study the impact of the force field parameters on aggregation characteristics like contact area and distance between platelets.

Measures and Formulas

The inter-platelet distance refers to the distance between the centers of mass of two platelets, and is calculated as:

$$x = \|\mathbf{r}_A - \mathbf{r}_B\|_2 \quad (6)$$

\mathbf{r}_A and \mathbf{r}_B are the centers of mass for platelets A (adhered to the wall) and B (recruited from flow), respectively.

TABLE 1. Parameters for aggregation model.

Key model parameters	Model values in DPD units	Model values in SI units	Key biophysical properties
r_0	0.38	67.5 nm	Equilibrium bond length for $\alpha\text{IIb}\beta\text{3-Fg-}\alpha\text{IIb}\beta\text{3}$ ¹⁰
r_c	0.5	87.5 nm	Calculated from $\alpha\text{IIb}\beta\text{3}$ extending above the surface and Fg ^{29,43}
α	1.0	$5.62 \mu\text{m}^{-1}$	Correlation with contact area from <i>in vitro</i> experiments (“Validation”)
D_0	10.0	$1.45 \times 10^{-19} \text{ J}$	Correlation with contact area from <i>in vitro</i> experiments (“Validation”)
f^A	10.0	0.82 pN	Correlation with AFM ²¹
Δt	2.5×10^{-5}	52 ps	Timestep size

To calculate the nearest distance, r_{ij} is computed between the i th particle on membrane platelet A and j th particle on membrane of platelet B,

$$d_{\min} = \min\{r_{ij} | r_{ij} = \|r_i - r_j\|_2, r_i \in M_A, r_j \in M_B\}. \quad (7)$$

M_A and M_B are the group of membrane particles for platelets A and B, respectively.

For calculating the contact area, we need a threshold value that defines aggregation contact area represented by each membrane particle. The threshold value (T_d) refers to the distance between platelet surface when a bond begins to form. The $\alpha\text{IIb}\beta\text{3}$ receptors extend about 20 nm above the surface^{29,43} and Fg is about 47.5 nm in molecular length.²⁰ The approximated distance between platelet surface at the time of aggregation is 87.5 nm.

We define the set of contact particles as:

$$C_{AB} = \left\{ r_i | r_{ij} < T_d, r_{ij} = \|r_i - r_j\|_2, r_i \in M_A, r_j \in M_B \right\} \quad (8)$$

Hence, contact area is defined as:

$$C_a = |C_{AB}| \cdot \frac{S}{|M|}, \quad (9)$$

where S is the surface area and M is the set of membrane particles of the platelet where $|\cdot|$ is the notation for cardinality of a set.

We use our simulations to calculate the detaching force and validate it with *in vitro* values. In our simulations, the detaching force is calculated as a multiple of rupture force per $\alpha\text{IIb}\beta\text{3-Fg}$ bond and number of bonds between platelets. The number of $\alpha\text{IIb}\beta\text{3}$ receptors in the contact region, assuming homogeneous distribution, is calculated from experimental observations. Given that only 10% of the number of $\alpha\text{IIb}\beta\text{3}$ receptors in the contact region may participate in bonding with Fg,³⁹ an approximate number of $\alpha\text{IIb}\beta\text{3-Fg}$ bonds between platelets is obtained.

Detaching force data is obtained from previously published²¹ rupture force for $\alpha\text{IIb}\beta\text{3-Fg}$ bonds obtained through Atomic force microscopy (AFM) experiments. AFM is a technique used to perform force spectroscopy and can measure precise bonding or adhesion forces at the single molecule level. The measured quantity is the rupture force with piconewton resolution.³ For measuring the rupture force between the $\alpha\text{IIb}\beta\text{3}$ and Fg bonds a bead coated with fibrinogen was trapped by a focused laser beam in a flow chamber and repeatedly brought in contact with purified $\alpha\text{IIb}\beta\text{3}$ immobilized on silica beads. Tension was produced when the bead was displaced from the laser focus until the $\alpha\text{IIb}\beta\text{3-fibrinogen}$ or $\alpha\text{IIb}\beta\text{3-fibrin}$ bond ruptured. This is a proxy for $\alpha\text{IIb}\beta\text{3}$ receptors on platelets interacting with fibrinogen. The applied force strength was then recorded as the rupture force for $\alpha\text{IIb}\beta\text{3}$ and Fg bonds. The detaching force range is calculated as multiples of the rupture force range for $\alpha\text{IIb}\beta\text{3}$ and Fg bonds (10.0–20.0 pN)²¹ obtained *in vitro* using AFM and approximate number of $\alpha\text{IIb}\beta\text{3-Fg}$ bonds.

Since aggregation is a dynamic phenomenon, we use RMSF to analyze differences in trajectory that arise from rigidity or deformability of the platelets and determine a stable state for aggregation. Specifically, RMSF is used to determine an average position about which the system may pose some small fluctuations. We calculate the RMSD (Root mean square deviation) and RMSF by the following formula:

$$\text{RMSF} = \sqrt{\frac{1}{N} \sum_{i=1}^N (r_i(t + \Delta t) - r_i(t))^2}, \quad (10)$$

where N is the number of particles whose positions are being compared and $r_i(t)$ is the position of particle i at time t .

From the massive amounts of data generated in the simulations we can calculate platelet force between two platelets generated by the accumulating pairwise force between the platelets. In this work we report the magnitude of aggregation force for every $0.104 \mu\text{s}$.

Unit Conversion

The model units are converted from dimensionless units to physical units.⁴⁸ The reference length $\sigma_r = \frac{D_\rho}{D_\rho^*}$, where $D_\rho = 4 \mu\text{m}$ and $D_\rho^* = 4$, the reference mass $m_r = \frac{\rho\sigma_r^3}{\rho^*}$ where the fluid density of plasma $\rho = 1060 \text{ kg/m}^3$ and the particle density $\rho^* = 3$. Reference units are presented in Table 2.

IN VITRO EXPERIMENTS

Whole blood, 30 mL, was obtained by antecubital venipuncture from consenting healthy adult volunteers as per a Stony Brook University IRB-approved protocol and anticoagulated with 10% ACD-A. Isolated platelets (GFP) and red blood cells (RBC) were prepared from whole blood as previously described.^{9,37} Flow-induced aggregation was initiated through a two-step process. First, $1 \times 10^5/\mu\text{l}$ GFP and RBCs (40% final concentration) were mixed in Hepes-buffered modified Tyrode's solution ("platelet buffer"). This mixture was perfused through a $0.1 \times 1 \text{ mm}$ microchannel (Luer VI^{0.1}, ibidi USA Inc., Fitchburg, WI) pre-coated with $100 \mu\text{g/mL}$ vWF at 15 dyne/cm^2 for 1 min using a syringe pump (NE-1010, New Era Pump Systems, Farmingdale, NY). The inclusion of RBCs promotes margination of platelets out of the core flow entering the microchannel and increases local platelet density. The GFP-RBC mixture was subsequently allowed to settle for 19 min to initiate adhesion of margined platelets to immobilized GFP. The residual GFP-RBC mixture was flushed gently with Tyrode's solution, after which a $1.5 \times 10^5/\mu\text{L}$ GFP solution mixed with 1.5 mg/mL fibrinogen was perfused at 6.7 dyne/cm^2 for up to 20 min. Platelet motion was captured at 200 fps on a Zyla sCMOS camera (Andor Technology, South Windsor, CT) mounted on an inverted DIC microscope with $100 \times$ oil immersion objectives (NA = 1.45, Eclipse Ti-E, Nikon Instruments Inc., Melville, NY). Exported images were analyzed for contact events, selected based on the interaction of individual discoid platelets. Using NIH ImageJ, a re-

gion of interest capturing the aggregation or recruitment event was smoothed using Gaussian blur, with contrast adjusted using a FFT-based bandpass filter. Platelet major and minor radii, center coordinates, and major axis rotation angles were measured from the ellipses bounding the contacting platelets. Ellipsoidal volume for each platelet was calculated using thickness approximated from platelets flipping under flow conditions. Contact area between two interacting platelets was calculated using a meshing approach, with the number of surface points within the intersection "contacting" threshold of the three-dimensional platelet models counted and multiplied by the unit surface area of each platelet to determine the inter-platelet contact area. Supplemental Material S1 shows platelet aggregation without any visible shape change and Supplemental Material S2 presents a histogram of contact area with mean and variance.

RESULTS

Using the model, we can investigate some pre-aggregation and aggregation characteristics, including the distance between platelets, approach speed, contact area and detaching force. We present these results and explore their dynamics in relation to our interplatelet force field.

Validation

Our aggregation model can predict the molecular level aggregation phenomena and clearly illustrate the microphenomena involved during the evolution of bond formations. Figure 3 shows the detaching force calculated for deformable platelets lies within the range of detaching force measured *in vitro*. In Fig. 4, mean contact area (measured when the platelets form a stable aggregate) from simulations is compared with the mean contact area measured from *in vitro* images ("In Vitro Experiments"). From the Supplemental Material S3 and Fig. 4 we can see the contact area between the platelets increases and then reaches a stable state. We simulate aggregation until the RMSF

TABLE 2. Reference units used in the model for unit conversions from dimensionless to SI units.

Terms	Symbol/formula	Model values	SI values	SI units
Length	σ_r	1	1.78×10^{-7}	m
Time	t_r	1	2.08×10^{-6}	s
Mass	m_r	1	1.99×10^{-18}	kg
Force	$\frac{m_r \sigma_r}{t_r^2}$	1	8.15×10^{-14}	N
Energy	$\frac{m_r \sigma_r^2}{t_r^2}$	1	1.45×10^{-20}	J
Velocity	$\frac{\sigma_r}{t_r}$	1	8.53×10^{-2}	m/s

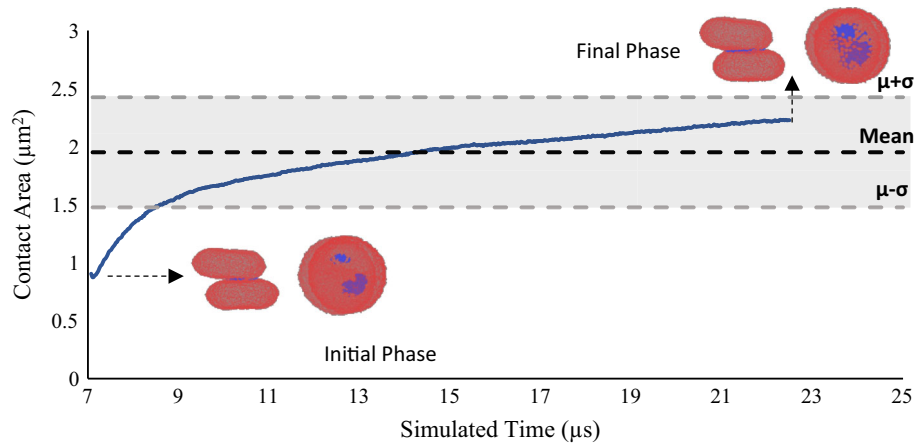


FIGURE 4. Contact area (μm^2) against simulated time (μs) for deformable platelets with $\alpha = 1.0$, $D_0 = 10.0$, $f^A = 10.0$. Mean shown is the mean contact area measured from *in vitro* experiments.

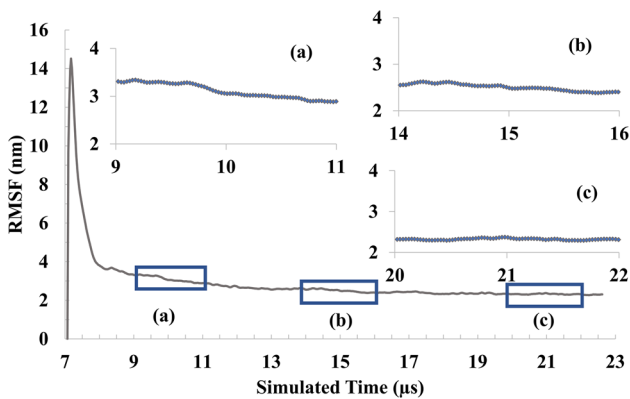


FIGURE 5. RMSF (window size $0.104 \mu\text{s}$, step size $0.26 \mu\text{s}$) of the recruited platelet.

of the recruited platelet is stable. Figure 5 presents RMSF of the recruited platelet averaged over $0.26 \mu\text{s}$. The figure also includes subplots (a), (b) and (c) showing the RMSF decreasing with time and possessing fewer fluctuations. Figure 12 presents the top view of contact area highlighted using blue color with simulated time. With this we can conclude that our model is in good agreement with the measured (i) contact area and (ii) detaching force.

Marginated Platelets

We calculate the nearest distance d_{\min} (as defined in “Measures and Formulas”) between the platelet membranes and present the change in platelet trajectory during the process of recruitment for different α . Figure 6 presents the evolution of d_{\min} vs. simulated time for three values of α values with $D_0 = 10.0$ and highlighting the threshold $T_d = 87.5 \text{ nm}$ (as defined in “Measures and Formulas”). From Fig. 6, we notice

that for each value of α , the nearest distance of the platelet before contact is characterized by a large drop which is depicted in the figure as a change of $1.2 \mu\text{m}$ before contact. As the flowing platelet comes in contact to the adhered platelet the trajectory becomes stable characterized by small fluctuations below the threshold value. Comparing the trajectory for the three α values we observe that the time to recruit a platelet from the free flow increases as the value of α increases. For $\alpha = 0.8$ it takes $0.83 \mu\text{s}$ which increases to $7 \mu\text{s}$ for $\alpha = 1.2$. Validating with the *in vitro* measurements, we found that $\alpha = 1.0$ with $D_0 = 10.0$ is the correct parameter set for the aggregation force field (see “Parameter Determination”). Therefore, our model predicts that the trajectory for recruitment is given by $\alpha = 1.0$ and time to recruit a platelet from flow is $2.29 \mu\text{s}$.

Figure 7 shows the approach speed of the platelets calculated using d_{\min} averaged over $0.52 \mu\text{s}$. We observe that as the value of α increases the peak approach speed decreases. For $\alpha = 0.8$, the peak approach is 254.3 cm/s which decreases to 142.2 cm/s for $\alpha = 1.2$. Figure 7 also presents a sequence of animation snapshots of platelets colored by velocity to illustrate the change in velocity while flowing in their recruitment trajectory. The sequences A, B, C present the evolution of recruitment for $\alpha = 0.8, 1.0, 1.2$ respectively. The subfigures A.2, B.2 and C.2 show the peak velocity for the respective α values at first contact with the adhered platelet. The difference in peak velocities is reflected in the moving platelet through the color bar. Figure 7 and Supplemental Material S4 show propagation of velocity in the recruited platelet from the point of contact to the furthest end. Using our model with the correct parameters, we predict that the value for the peak speed is 102.3 cm/s and the evolution of speed is given by $\alpha = 1.0$ during the recruitment process.

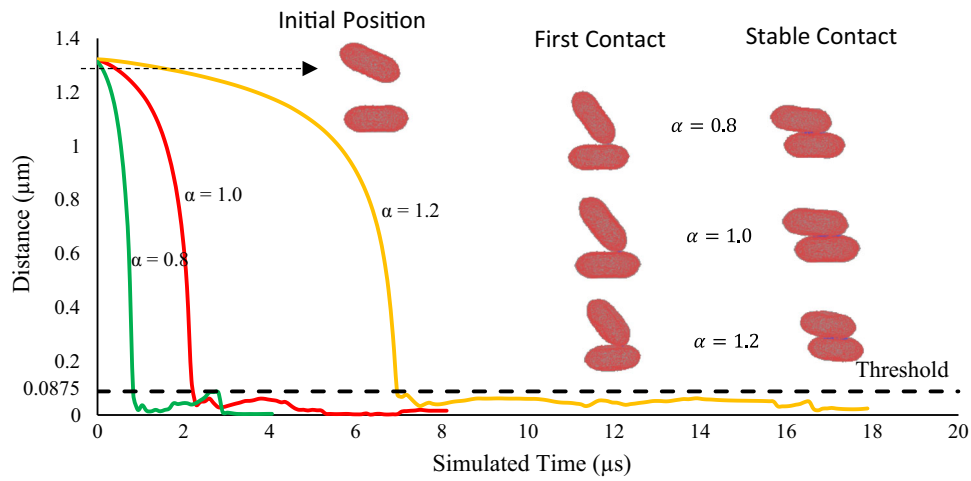


FIGURE 6. Minimum distance (μm^2) between the platelet membranes during the process of recruitment vs. simulated time (μs).

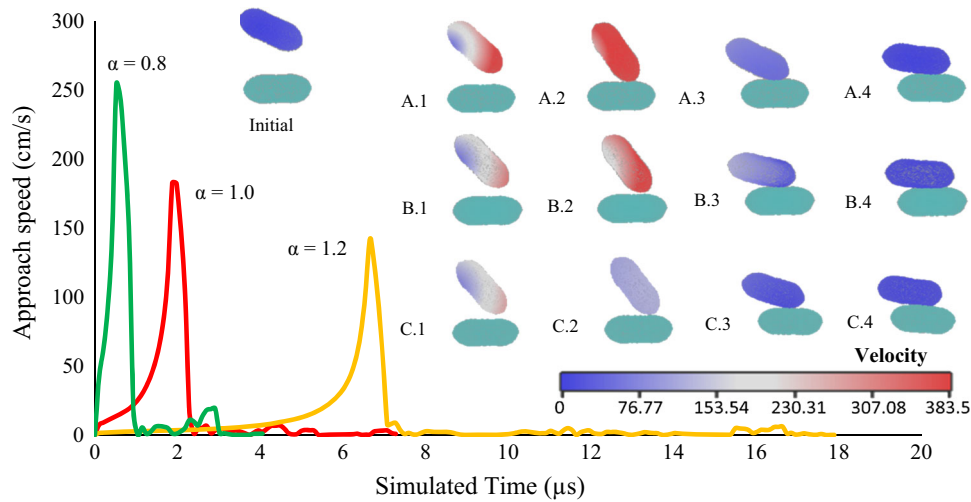


FIGURE 7. Approach speed (cm/s) against simulated time (μs).

Finally, we calculate force between platelets when the recruited platelet approaches the platelet adhered to the wall. Figure 8 presents the force between platelets against the simulated time for different values of α with $D_0 = 10.0$. This force is between the platelets because of the applied force field. Using parameters found in “Parameter Determination”, it can be inferred that the evolution of force between platelets for recruitment given by $\alpha = 1.0$ finds the balance between the attractive and repulsive forces. These observations reflect the impact of α during the recruitment process.

By analyzing measured forces between aggregating platelets due to the $\alpha\text{IIb}\beta 3\text{-Fg-}\alpha\text{IIb}\beta 3$ bond, we discover the model of the recruiting force as a function of inter-platelet distance x as follows:

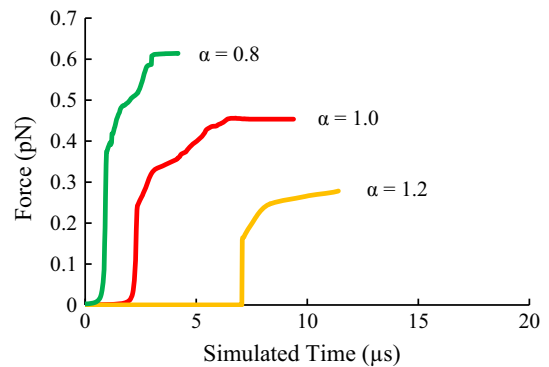


FIGURE 8. Force (pN) between two platelets against simulated time (μs).

$$\begin{aligned}
F(x) &= S(x) \cdot M(x) - (1 - S(x)) \cdot H(x) \\
&= S(x) \cdot F_0 \exp(-\beta(x - x_b)) - (1 - S(x)) \\
&\quad \cdot k_b(x - x_b)
\end{aligned} \quad (11)$$

where

$$S(x) = \frac{1}{1 - \exp(50(x - 2.345))}$$

In this equation, x is the inter-platelet distance as defined in “Measures and Formulas”. The term $M(x)$ presents the Morse-like non-bonded interaction that usually dominates in long-medium range distance. The term $H(x)$ is the Hooke-like bonded interaction and describes the impact of α IIB β 3-Fg- α IIB β 3 bonds that occur during platelet aggregation under low shear flow. $S(x)$ reflects the smoothed transition from margined effect to bond-mediated aggregation.

Table 3 presents the parameters for recruitment force derived using our model. The model given in Eq. (11) modifies the previous models that only rely on Morse terms by incorporating the previously-neglected effect of molecular-scale bonds, thus improving the accuracy of describing the recruitment with molecular details.

Figure 9 presents the force against the center distance x (as defined in “Measures and Formulas”) for $\alpha = 1.0$ and $D_0 = 10.0$. Since force during recruit-

TABLE 3. Parameters for recruitment force model given by Eq. (1).

Model parameters	DPD	SI
β	0.82	$4.6590 (\mu\text{m})^{-1}$
F_0	1.93×10^{-2}	$8.86 \times 10^{-3} \text{ pN } (\mu\text{m})^{-1}$
x_b	17.3	$3.070 \mu\text{m}$
k_b	0.723	$3.316 \text{ pN } (\mu\text{m})^{-1}$

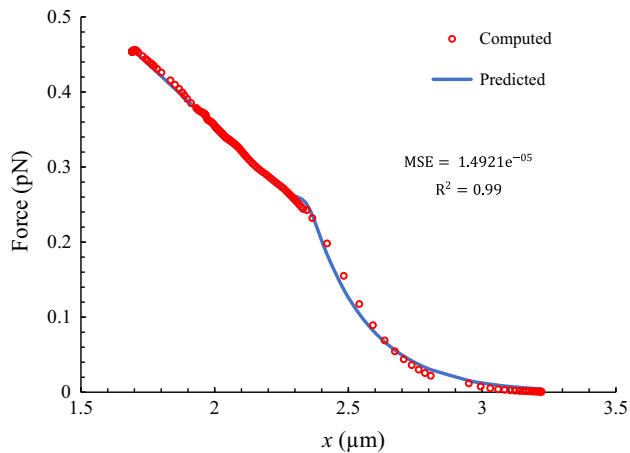


FIGURE 9. Force (pN) as a function of distance between platelet centers (μm).

ment cannot be measured directly from the *in vitro* images, this function, determined using particle level details, can directly provide the force by using the distance between platelet centers from *in vitro* images without going through the complex and expensive process of modeling.

Contact Area and Detaching Force

We predict the contact area between platelets using Eqs. (8) and (9). Figure 10 presents the contact area (μm^2) between platelets against simulated time (μs) during recruitment aggregation. From Fig. 10 we can observe three different phases of aggregation during the evolution of contact area. In the first phase of recruitment, contact area increases rapidly, and the recruited platelet adjusts its position by sliding on the adhered platelet, thereby finding the optimal position for contact. We refer to this phase as the positional adjustment phase of aggregation and bonds are formed and broken as one platelet slides on the other. This positional adjustment leads to a rapid increase in contact area, and dynamic bonding and debonding leads to fluctuations in the contact area curve during the positional adjustment phase. From Fig. 10, we can see that this phase lasts for about $5 \mu\text{s}$.

In the second phase, larger number of new bonds are formed than are broken. We refer to this phase as the bond formation phase, wherein bond formation becomes more prominent and few bonds are broken. This is demonstrated through the consistent growth of contact area, which possesses significant increments since the platelet receptors engage in aggressive bond formation with Fg. This phase takes about $6 \mu\text{s}$ to complete.

In the third phase, contact area stabilizes with time, possessing very small increment area during the last two μs . This can also be affirmed from RMSF in Fig. 5. We refer to this phase as the equilibrium phase. Correlating this evolution of contact area with evolution of detaching force during different phases of aggregation, Fig. 11 shows how initially formed bonds become permanent over time and form a stable aggregate. During these phases, contact area and detaching force have a linear relationship.

The evolution of contact area through the three phases (Supplemental Materials S3 and S4) demonstrates that aggregation begins with transient bond formation, but with time as adjustment of contact position concludes, bond formation stabilizes, and more permanent bonds are formed finally leading to a stable aggregate. The slow sliding movement of the flowing platelet over the adhered platelet agreed with the microphenomena observed *in vitro* (Supplemental Material S1).

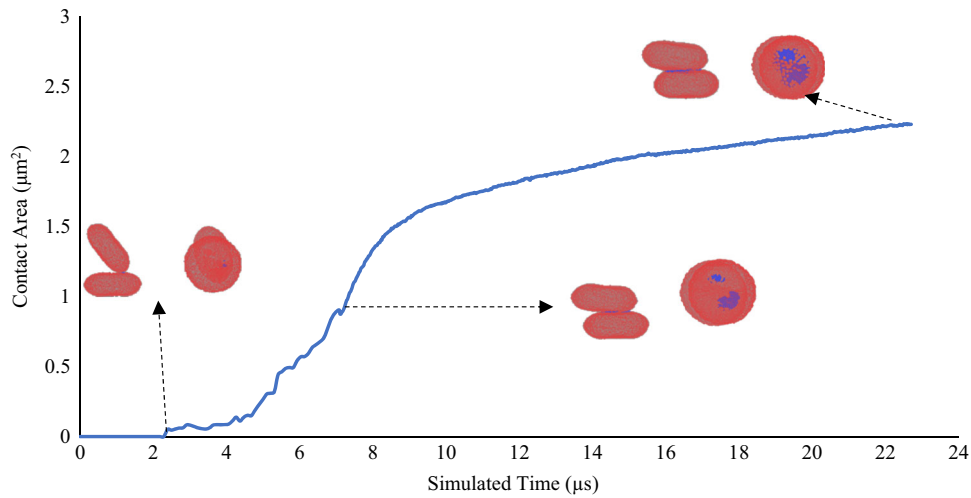


FIGURE 10. Evolution of Contact Area (μm^2) with simulated time (μs) illustrating first contact and final contact through the side and top view.

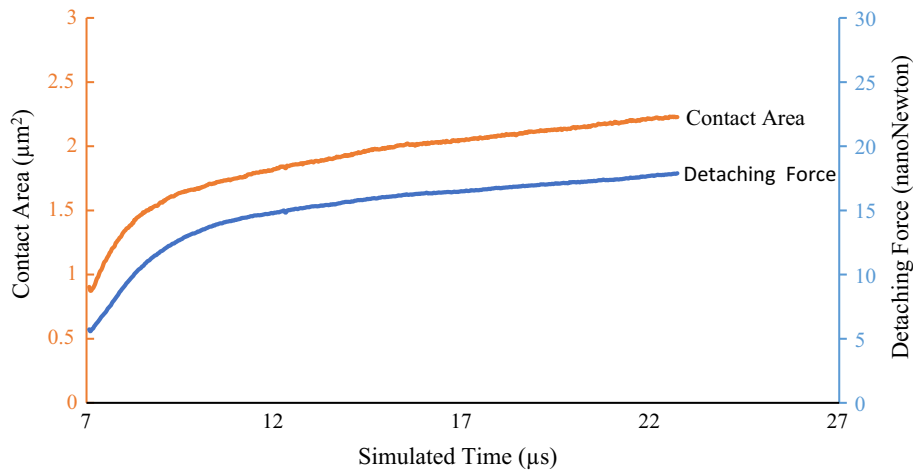


FIGURE 11. Contact Area (μm^2) (left axis) and Detaching Force (nanoNewton) against simulated time (μs).

Figure 9 presents the detaching force for different values of f^A (DPD units) using the deformable platelet model. The range of detaching force obtained from the AFM experiments²¹ (“Measures and Formulas”) is indicated with the grey highlighted area. With the increase in f^A number of bonds formed between the platelets increases. A quadratic polynomial can be used to approximate total detaching force as a function of f^A . The function is given by

$$F_{\text{detach}} = 8.4241 \exp(0.0365f^A), \quad (12)$$

where $f^A \in [0.1, 100]$. Figure 11 presents detaching force evolution with time. We observe that there is an initial spike in bond formation after which bond formation stabilizes and very few new bonds are formed.

Rigid and Deformable Platelets

We compare our recruitment aggregation model for deformable and rigid platelets. The rigid platelet model adapts the same platelet model but with a rigid constraint. Both models use the same parameter set as presented in Table 1. We compare our aggregation model with rigid platelets with the *in vitro* experiments and confirm that the rigid platelets underestimate the final contact area by 89% and detaching force by 91–93%. Our aggregation model with deformable platelets can reproduce the correct range of contact area and detaching force.

Table 4 compares contact area and detaching force for rigid and deformable platelets calculated from simulations and obtained *in vitro*. This shows that a

TABLE 4. Comparison of rigid and deformable platelets.

Parameters	Rigid platelets	Deformable platelets	<i>In vitro</i> results
Contact area (μm^2)	0.213 ± 0.001	2.227 ± 0.003	1.950 ± 0.484
Detaching force (nN)	0.844 ± 0.007	17.842 ± 0.027	9.100 ~ 18.200

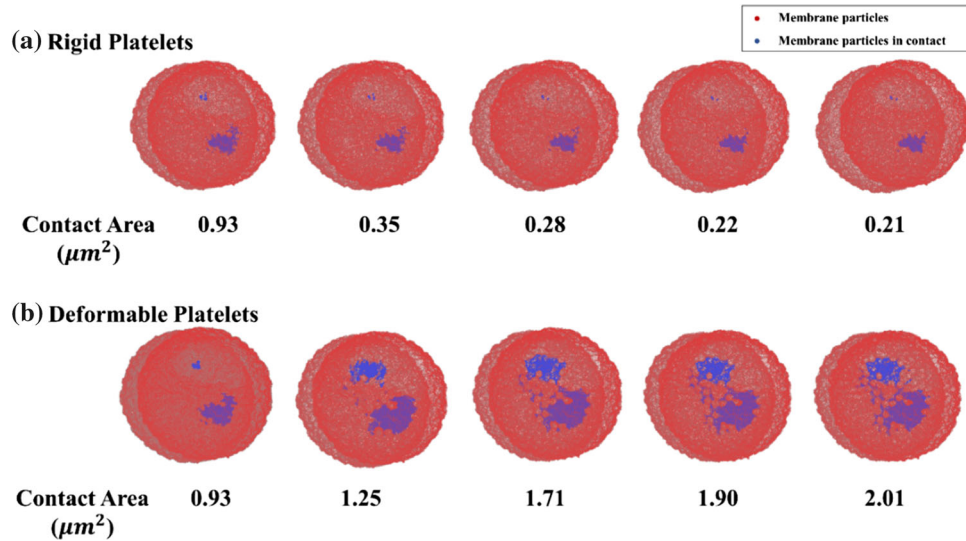


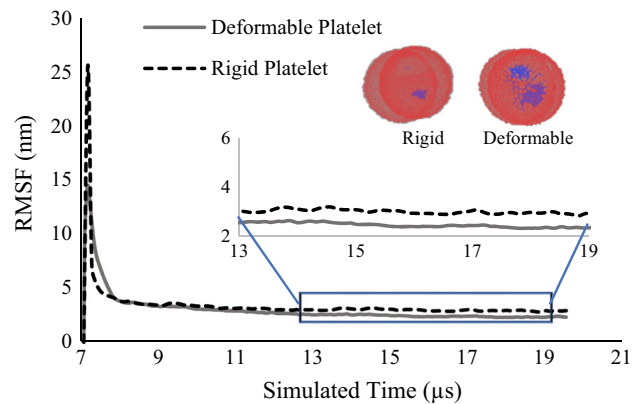
FIGURE 12. Comparison between aggregation contact area for rigid and deformable models.

rigid constraint, although simplifies the modeling, significantly underestimates aggregation strength. Figure 12 illustrates the contact area difference between the rigid and deformable platelets through top view snapshots of the aggregating platelets. The blue particles in the figure represent particles that have formed a bond.

A comparative chart for RMSF is presented for both models in Fig. 13. It is observed that the RMSF is stable for the deformable model and is characterized by more fluctuations as compared to the deformable platelet model. This shows that aggregation in deformable platelet is consistently stable compared to rigid platelets. Due to lower contact area and lower rate of bond formation rigid platelets have a lower order of attachment and are more likely to form transient aggregates under shear flows.

These results lead us to following observations:

- Rigid platelets in the aggregation model lead to a very significant underestimation of the contact area by 89% and detaching force by 91–93%.
- In the equilibrium state, the deformable model is more stable than the rigid model under shear flows. Hence, rigid platelet aggregates are unstable and more likely to detach.

FIGURE 13. RMSF (window size $0.104 \mu\text{s}$, step size $0.26 \mu\text{s}$) comparison.

Therefore, neglecting deformability may lead to erroneous predications of aggregation properties.

DISCUSSION AND FUTURE WORK

We developed the first multiscale model of platelet recruitment and aggregation under flow that includes bonding receptors on the platelet membrane surface

and responds to extracellular stress.⁴⁸ We applied it to study recruitment aggregation of unactivated platelet by a platelet already attached to a vascular wall at molecular levels. A hybrid force field is designed to describe the bonded and nonbonded interactions between the platelets. A complete parameter sensitivity study for force field parameters was performed. This model can accurately describe the target aggregation characteristics including contact area and detaching force. Deformable platelets have higher contact area has been quantitatively demonstrated at the micro-scales. Even though experiments for thrombus formation have been conducted in the past, there is scarcity of literature on platelet aggregation. This model fills the gap that is present in platelet aggregation data at microscales. This is the first work that corroborates *in silico* and *in vitro* results of contact area and detaching force while quantifying the effect of platelet deformability on aggregation characteristics.

The Morse potential has been used to model the interaction of cells including platelets.^{45,47} Although Morse potential can model the microscale properties of these interactions,⁴⁵ it did not simulate the molecular bond formation required for aggregation. We followed the approach of Ref. 45 using Morse potential for modeling the recruitment of marginated platelet in the cell free layer. Importantly, we improved this force field for modeling aggregation at microscales by adding a Hooke's term for precisely modeling the receptor–ligand interaction in low shear flows. With this improvement, the aggregation model possesses an added ability of illustrating the microphenomena that otherwise have been missing.^{41,42,45}

It has been demonstrated in the past^{23,35,36} that with the change in vasculature and shear stress conditions, the receptor and ligands involved in aggregation change. It is critical that any aggregation/adhesion model reflects these molecular-level changes induced by macro-level phenomena. Past numerical aggregation studies have validated their models at macroscales using collision characteristics^{26,27} or growth rate of thrombus.⁴⁵ These models, though versatile in conditions and shear stress ranges, lack the validation of the receptor–ligand bond role in aggregation at the molecular level. In this work, the aggregation model is directly validated with *in vitro* measurements at two scales. The micro-level phenomena are validated using the contact area and the nanoscale bond properties are validated using detaching force. This is the first work that validates the receptor–ligand bonding with AFM-based rupture forces.

Contact area is measured from the simulations and compared with the *in vitro* measurements. Given the limitation of the Zyla sCMOS camera (temporal resolution of 200 fps and spatial resolution of 0.07 $\mu\text{m}/\text{px}$

at the settings used for *in vitro* experiments) and inverted DIC microscope utilized, contact area is the only measure that can be directly and reliably quantified from experimental images. The simulations illustrate the evolution of contact area and inform the phenomena that happen at microscale during aggregation. Through this evolution at microscales, we discover the different phases of aggregation dynamics. Each of these phases characterizes a unique aspect of the platelet recruitment process. In the positional adjustment phase, platelets go through dynamic bond formation and breakage. In the bond formation phase, stable bond formation begins, and few bonds are broken. In the equilibrium phase, the bonds are stabilized while no significant change in contact area is observed. Thus, the model's ability to quantify and predict aggregation characteristics that cannot be reliably measured *in vitro* is an advancement for exploring molecular level details.

Rupture force validation was performed using the detaching force for determining f^A in the Hooke's term. The detaching force and its time-varying behavior during aggregation, is obtained from the simulations. The evolution of detaching force during the different phases shows the growth and stabilization of bond formation, and detaching force and contact area is characterized by a linear relationship. This shows that contact area is proportionately influenced by the bond formation, thus emphasizing the importance of the use of detaching force for determining f^A in this model.

Minimum distance and approach speed calculated from the simulations predict microscale details about the marginated platelets. The relationship between the model parameters and their impact on the trajectory of the marginated platelet provides a detailed understanding of the recruitment process. Using parameters determined in “[Parameter Determination](#)”, we calculate the trajectory for the recruited platelet and the evolution of approaching speed and force during the recruitment process. At the beginning of the recruitment, the trajectory of the flowing platelet is steep and approaching speed increases rapidly. At the time of first contact, minimum distance falls below threshold and approaching speed peaks. After the first contact, the minimum distance and approaching speed stabilize.

The force between the marginated platelets in the cell free layer was calculated. We formulated a function for predicting microscale level force during recruitment using macroscale quantities like inter-platelet distance. In the function given by Eq. (11), the exponential term and linear terms are connected using a sigmoid function. The sigmoid function models the smooth transition of a platelet from free flow in the

cell-free layer to bond formation. Previous models, using only Morse potential for modeling platelet aggregation, miss the dynamics of the receptor–ligand binding. Our model, augmenting the Morse force field by a Hooke’s term, encapsulates the transition from margination to initiation of aggregation through formation of receptor–ligand bonds.

For simplifying modeling and saving computational costs, platelets are often modeled as rigid bodies.^{25–27,45} Previous works have studied the effects of rigidity assumption on platelets and determined that it may lead to erroneous predictions.²² The effect of a rigidity constraint on a platelet model was examined using this setup for aggregation. In this approach, rigidity was added to the platelets and key target properties were compared with the *in vitro* results. We confirmed that the rigid model underestimates the contact area and detaching force. Using RMSF, it was observed that rigid platelets form unstable aggregates. Although platelets are less deformable than RBCs, this work demonstrates that a rigidity assumption is erroneous. Error in estimation of contact characteristics may propagate in thrombus modeling using rigid platelets, thus leading to underestimation of thrombus growth.

Our model with adjustable parameters can be adapted to different ranges of shear stress by incorporating equilibrium bond length for a pair of receptor and ligand. For example, for pathological shear stress as high as 80 dyne/cm², aggregation is mediated by GPIb and vWF and the GPIb–vWF equilibrium bond length is used to determine r_0 and r_c . As shown in our previous work, our platelet model can be modified to consider high shear stress to simulate aggregation in such pathological conditions.⁴⁶

Aggregation in free flows and adhesion to the vascular wall can be developed using the same principles. In future studies, a platelet-mediated thrombus growth model under shear will be developed. This thrombus model will adapt the molecular-scale properties of our current recruitment aggregation model, thus predicting macro-scale properties using micro-scale principles. Such a model will have the advantage of reflecting molecular level changes in receptor–ligand bond formation. We expect our multiscale model to be adopted by other fields such as drug design by considering the impact of mechanical events triggering biochemical responses. Our model can be used for systems pharmacology models in drug development and delivery. The prediction capability of our model can enable manipulation of transmembrane aggregation receptors *via* pharmacologic or biochemical agents by changing their modeling parameters or blocking them completely, manipulating platelet membrane proper-

ties—e.g. fluidity, and modulating the model cytoskeletal properties and activation dynamics.

ELECTRONIC SUPPLEMENTARY MATERIAL

The online version of this article (<https://doi.org/10.1007/s12195-019-00583-2>) contains supplementary material, which is available to authorized users.

ACKNOWLEDGEMENTS

This publication was made possible by grants from the National NIH U01 HL131052-014 (PI: Danny Bluestein, Co-Investigators: Yuefan Deng, Marvin J. Slepian). The simulations in this study used the XSEDE computing resource award DMS150011 at the SDSC Comet supercomputer (PI: Peng Zhang) and LI-Red supercomputer, Stony Brook University.

CONFLICT OF INTEREST

Prachi Gupta, Peng Zhang, Jawaad Sherif, Danny Bluestein and Yuefan Deng declare that they have no conflict of interest.

HUMAN STUDIES

All procedures followed were in accordance with the ethical standards of the responsible committee on human experimentation (institutional and national) and with the Helsinki Declaration of 1975, as revised in 2000 (5). Informed consent was obtained from all patients for being included in the study. No animal studies were carried out by the authors for this article.

REFERENCES

- Benjamin, E. J., S. S. Virani, C. W. Callaway, A. M. Chamberlain, A. R. Chang, S. Cheng, S. E. Chiuve, M. Cushman, F. N. Delling, R. Deo, S. D. de Ferranti, J. F. Ferguson, M. Fornage, C. Gillespie, C. R. Isasi, M. C. Jimenez, L. C. Jordan, S. E. Judd, D. Lackland, J. H. Lichtman, L. Lisabeth, S. Liu, C. T. Longenecker, P. L. Lutsey, J. S. Mackey, D. B. Matchar, K. Matsushita, M. E. Mussolino, K. Nasir, M. O’Flaherty, L. P. Palaniappan, A. Pandey, D. K. Pandey, M. J. Reeves, M. D. Ritchey, C. J. Rodriguez, G. A. Roth, W. D. Rosamond, U. K. A. Sampson, G. M. Satou, S. H. Shah, N. L. Spartano, D. L. Tirschwell, C. W. Tsao, J. H. Voeks, J. Z. Willey, J. T. Wilkins, J. H. Wu, H. M. Alger, S. S. Wong, P. Muntner, and E. American Heart Association Council on, C. Prevention Statistics, and S. Stroke Statistics. Heart disease and stroke statistics-2018 update: a report from the

- American Heart Association. *Circulation*. 137:e67–e92, 2018.
- ²Campbell, R. A., M. Aleman, L. D. Gray, M. R. Falvo, and A. S. Wolberg. Flow profoundly influences fibrin network structure: implications for fibrin formation and clot stability in haemostasis. *Thromb. Haemost.* 104:1281–1284, 2010.
 - ³Carvalho, F. A., and N. C. Santos. Atomic force microscopy-based force spectroscopy-biological and biomedical applications. *IUBMB Life* 64:465–472, 2012.
 - ⁴Espanol, P., and P. Warren. Statistical mechanics of dissipative particle dynamics. *Europhys. Lett.* 30:191, 1995.
 - ⁵Fedosov, D. A., and G. E. Karniadakis. Triple-decker: interfacing atomistic-mesoscopic-continuum flow regimes. *J. Comput. Phys.* 228:1157–1171, 2009.
 - ⁶Fogelson, A. L. Continuum models of platelet-aggregation: formulation and mechanical-properties. *SIAM J. Appl. Math.* 52:1089–1110, 1992.
 - ⁷Frojmovic, M. M. Flow cytometric analysis of platelet activation and fibrinogen binding. *Platelets* 7:9–21, 1996.
 - ⁸Gao, C., P. Zhang, G. Marom, Y. F. Deng, and D. Bluestein. Reducing the effects of compressibility in DPD-based blood flow simulations through severe stenotic microchannels. *J. Comput. Phys.* 335:812–827, 2017.
 - ⁹Girdhar, G., M. Xenos, Y. Alemu, W. C. Chiu, B. E. Lynch, J. Jesty, S. Einav, M. J. Slepian, and D. Bluestein. Device thrombogenicity emulation: a novel method for optimizing mechanical circulatory support device thromboresistance. *PLoS ONE* 7:e32463, 2012.
 - ¹⁰Goldsmith, H. L., F. A. McIntosh, J. Shahin, and M. M. Frojmovic. Time and force dependence of the rupture of glycoprotein IIb–IIIa-fibrinogen bonds between latex spheres. *Biophys. J.* 78:1195–1206, 2000.
 - ¹¹Groot, R. D., and P. B. Warren. Dissipative particle dynamics: bridging the gap between atomistic and mesoscopic simulation. *J. Chem. Phys.* 107:4423–4435, 1997.
 - ¹²Haga, J. H., A. J. Beaudoin, J. G. White, and J. Strony. Quantification of the passive mechanical properties of the resting platelet. *Ann. Biomed. Eng.* 26:268–277, 1998.
 - ¹³Huang, P. Y., and J. D. Hellums. Aggregation and disaggregation kinetics of human blood platelets: Part I. Development and validation of a population balance method. *Biophys. J.* 65:334–343, 1993.
 - ¹⁴Huang, P. Y., and J. D. Hellums. Aggregation and disaggregation kinetics of human blood platelets: part II. Shear-induced platelet aggregation. *Biophys. J.* 65:344–353, 1993.
 - ¹⁵Huang, P. Y., and J. D. Hellums. Aggregation and disaggregation kinetics of human blood platelets: part III. The disaggregation under shear stress of platelet aggregates. *Biophys. J.* 65:354–361, 1993.
 - ¹⁶Jackson, S. P. The growing complexity of platelet aggregation. *Blood* 109:5087–5095, 2007.
 - ¹⁷Jackson, S. P., W. S. Nesbitt, and E. Westein. Dynamics of platelet thrombus formation. *J. Thromb. Haemost.* 7(Suppl 1):17–20, 2009.
 - ¹⁸Lakes, R. Materials science: a broader view of membranes. *Nature* 414:503–504, 2001.
 - ¹⁹Leiderman, K., and A. L. Fogelson. Grow with the flow: a spatial-temporal model of platelet deposition and blood coagulation under flow. *Math. Med. Biol.* 28:47–84, 2011.
 - ²⁰Liang, X. M., S. J. Han, J. A. Reems, D. Gao, and N. J. Sniadecki. Platelet retraction force measurements using flexible post force sensors. *Lab. Chip.* 10:991–998, 2010.
 - ²¹Litvinov, R. I., D. H. Farrell, J. W. Weisel, and J. S. Bennett. The platelet integrin alphaIIb beta3 differentially interacts with fibrin versus fibrinogen. *J. Biol. Chem.* 291:7858–7867, 2016.
 - ²²Martinez, E. J., Y. Lanir, and S. Einav. Effects of contact-induced membrane stiffening on platelet adhesion. *Bio-mech. Mod. Mechanobiol.* 2:157–167, 2004.
 - ²³Maxwell, M. J., E. Westein, W. S. Nesbitt, S. Giuliano, S. M. Dopheide, and S. P. Jackson. Identification of a 2-stage platelet aggregation process mediating shear-dependent thrombus formation. *Blood* 109:566–576, 2007.
 - ²⁴Michelson, A. D. Platelets (3rd ed.). Cambridge: Academic Press, 2013.
 - ²⁵Mody, N. A., and M. R. King. Three-dimensional simulations of a platelet-shaped spheroid near a wall in shear flow. *Phys. Fluids*. 17:113302, 2005.
 - ²⁶Mody, N. A., and M. R. King. Platelet adhesive dynamics. Part I: Characterization of platelet hydrodynamic collisions and wall effects. *Biophys. J.* 95:2539–2555, 2008.
 - ²⁷Mody, N. A., and M. R. King. Platelet adhesive dynamics. Part II: high shear-induced transient aggregation via GPIIb/IIIa-vWF-GPIIb/IIIa bridging. *Biophys. J.* 95:2556–2574, 2008.
 - ²⁸Nesbitt, W. S., E. Westein, F. J. Tovar-Lopez, E. Tolouei, A. Mitchell, J. Fu, J. Carberry, A. Fouras, and S. P. Jackson. A shear gradient-dependent platelet aggregation mechanism drives thrombus formation. *Nat. Med.* 15:665–673, 2009.
 - ²⁹Parise, L. V., and D. R. Phillips. Reconstitution of the purified platelet fibrinogen receptor. Fibrinogen binding properties of the glycoprotein IIb–IIIa complex. *J. Biol. Chem.* 260:10698–10707, 1985.
 - ³⁰Pivkin, I. V., P. D. Richardson, and G. Karniadakis. Blood flow velocity effects and role of activation delay time on growth and form of platelet thrombi. *Proc. Natl. Acad. Sci. USA* 103:17164–17169, 2006.
 - ³¹Pivkin, I., P. Richardson, and G. Karniadakis. Effect of red blood cells on platelet aggregation. *IEEE Eng. Med. Biol. Mag.* 28:32–37, 2009.
 - ³²Plimpton, S., A. Thompson, and P. Crozier. LAMMPS Molecular Dynamics Simulator. <http://lammps.sandia.gov>, 2012.
 - ³³Pothapragada, S., P. Zhang, J. Sheriff, M. Livelli, M. J. Slepian, Y. Deng, and D. Bluestein. A phenomenological particle-based platelet model for simulating filopodia formation during early activation. *Int. J. Numer. Method Biomed. Eng.* 31:e02702, 2015.
 - ³⁴Qiu, Y., J. Ciciliano, D. R. Myers, R. Tran, and W. A. Lam. Platelets and physics: how platelets “feel” and respond to their mechanical microenvironment. *Blood Rev.* 29:377–386, 2015.
 - ³⁵Ruggeri, Z. M. Von Willebrand factor, platelets and endothelial cell interactions. *J. Thromb. Haemost.* 1:1335–1342, 2003.
 - ³⁶Ruggeri, Z. M., J. N. Orje, R. Habermann, A. B. Federici, and A. J. Reininger. Activation-independent platelet adhesion and aggregation under elevated shear stress. *Blood* 108:1903–1910, 2006.
 - ³⁷Sheriff, J., J. S. Soares, M. Xenos, J. Jesty, M. J. Slepian, and D. Bluestein. Evaluation of shear-induced platelet activation models under constant and dynamic shear stress loading conditions relevant to devices. *Ann. Biomed. Eng.* 41:1279–1296, 2013.
 - ³⁸Shiozaki, S., S. Takagi, and S. Goto. Prediction of molecular interaction between platelet glycoprotein Iba1 and von Willebrand factor using molecular dynamics simulations. *J. Atheroscler. Thromb.* 23:455–464, 2016.

- ³⁹Smyth, S. S., and L. V. Parise. Regulation of ligand binding to glycoprotein IIb–IIIa (integrin alpha IIb beta 3) in isolated platelet membranes. *Biochem. J.* 292(Pt 3):749–758, 1993.
- ⁴⁰Soares, J. S., C. Gao, Y. Alemu, M. Slepian, and D. Bluestein. Simulation of platelets suspension flowing through a stenosis model using a dissipative particle dynamics approach. *Ann. Biomed. Eng.* 41:2318–2333, 2013.
- ⁴¹Tosenberger, A., F. Ataulakhanov, N. Bessonov, M. Pantelev, A. Tokarev, and V. Volpert. The role of platelets in blood coagulation during thrombus formation in flow. *HAL*. 2012.
- ⁴²Tosenberger, A., F. Ataulakhanov, N. Bessonov, M. Pantelev, A. Tokarev, and V. Volpert. Modelling of thrombus growth and growth stop in flow by the method of dissipative particle dynamics. *Russ. J. Numer. Anal. Math.* 27:507–522, 2012.
- ⁴³Weisel, J. W., C. Nagaswami, G. Vilare, and J. S. Bennett. Examination of the platelet membrane glycoprotein IIb–IIIa complex and its interaction with fibrinogen and other ligands by electron microscopy. *J. Biol. Chem.* 267:16637–16643, 1992.
- ⁴⁴Willemsen, S. M., H. C. J. Hoefsloot, and P. D. Iedema. No-slip boundary condition in dissipative particle dynamics. *Int. J. Mod. Phys. C* 11:881–890, 2000.
- ⁴⁵Yazdani, A., H. Li, J. D. Humphrey, and G. E. Karniadakis. A general shear-dependent model for thrombus formation. *PLoS Comput. Biol.* 13:e1005291, 2017.
- ⁴⁶Zhang, P., C. Gao, N. Zhang, M. J. Slepian, Y. F. Deng, and D. Bluestein. Multiscale particle-based modeling of flowing platelets in blood plasma using dissipative particle dynamics and coarse grained molecular dynamics. *Cell. Mol. Bioeng.* 7:552–574, 2014.
- ⁴⁷Zhang, J., P. C. Johnson, and A. S. Popel. Red blood cell aggregation and dissociation in shear flows simulated by lattice Boltzmann method. *J. Biomech.* 41:47–55, 2008.
- ⁴⁸Zhang, P., L. Zhang, M. J. Slepian, Y. Deng, and D. Bluestein. A multiscale biomechanical model of platelets: correlating with in vitro results. *J. Biomech.* 50:26–33, 2017.

Publisher's Note Springer Nature remains neutral with regard to jurisdictional claims in published maps and institutional affiliations.